

Geophysical Research Letters°



RESEARCH LETTER

10.1029/2023GL104358

Key Points:

- Inverse temperature layer (ITL)
 allows transfer of heat from water into
 atmosphere.
- ITL has prounced diurnal seasonal cycles persisting year-around
- Water surface heat flux is simulated using non-gradient models

Supporting Information:

Supporting Information may be found in the online version of this article.

Correspondence to:

J. Wang, jingfeng.wang@ce.gatech.edu

Citation:

Wang, J., Liu, H., & Shen, L. (2023). An observational and modeling study of inverse-temperature layer and water surface heat flux. *Geophysical Research Letters*, 50, e2023GL104358. https://doiorg/10.1029/2023GL104358

Received 29 APR 2023 Accepted 6 JUL 2023

Author Contributions:

Conceptualization: Jingfeng Wang Data curation: Heping Liu Formal analysis: Jingfeng Wang Funding acquisition: Jingfeng Wang, Heping Liu, Lian Shen Investigation: Jingfeng Wang, Heping

Liu, Lian Shen

Methodology: Jingfeng Wang Project Administration: Jingfeng Wang Resources: Jingfeng Wang, Heping Liu, Lian Shen

Supervision: Jingfeng Wang Validation: Jingfeng Wang Visualization: Jingfeng Wang, Lian Shen Writing – original draft: Jingfeng Wang Writing – review & editing: Jingfeng Wang, Heping Liu, Lian Shen

© 2023. The Authors.

This is an open access article under the terms of the Creative Commons Attribution-NonCommercial-NoDerivs License, which permits use and distribution in any medium, provided the original work is properly cited, the use is non-commercial and no modifications or adaptations are made.

An Observational and Modeling Study of Inverse-Temperature Layer and Water Surface Heat Flux

Jingfeng Wang¹, Heping Liu², and Lian Shen³

¹School of Civil and Environmental Engineering, Georgia Institute of Technology, Atlanta, GA, USA, ²Department of Civil and Environmental Engineering, Washington State University, Pullman, WA, USA, ³Department of Mechanical Engineering and St. Anthony Falls Laboratory, University of Minnesota, Minneapolis, MN, USA

Abstract An "inverse-temperature layer" (ITL) of water temperature increasing with depth is predicted based on physical principles and confirmed by in situ observations. Water temperature and other meteorological data were collected from a fixed platform in the middle of a shallow inland lake. The ITL persists year-around with its depth on the order of one m varying diurnally and seasonally and shallower during daytimes than nighttimes. Water surface heat flux derived from the ITL temperature distribution follows the diurnal cycle of solar radiation up to 300 W m⁻² during daytime and down to 50 W m⁻² during nighttime. Solar radiation attenuation in water strongly influences the ITL dynamics and water surface heat flux. Water surface heat flux simulated by two non-gradient models independent of temperature gradient, wind speed and surface roughness using the data of surface temperature and solar radiation is in close agreement with the ITL based estimates.

Plain Language Summary Heat stored in water bodies resulting from the absorption of solar radiation is the energy supply of evaporation and sensible heat flux into the atmosphere from water surface. Transfer of the thermal energy from water body into the atmosphere is only possible when water temperature increasing with depth within the top water layer referred to as the "inverse temperature layer (ITL)." The existence and persistence of the theoretically predicted phenomenon are demonstrated by the field observations of water temperature profile at an inland lake. The ITL depth is found to be comparable to the penetration depth of solar radiation with evident diurnal and seasonal cycles following closely those of solar radiation. Further understanding and analysis of the ITL process require higher resolution data of water temperature and solar radiation profiles within the top-layer than those commonly collected in previous field experiments.

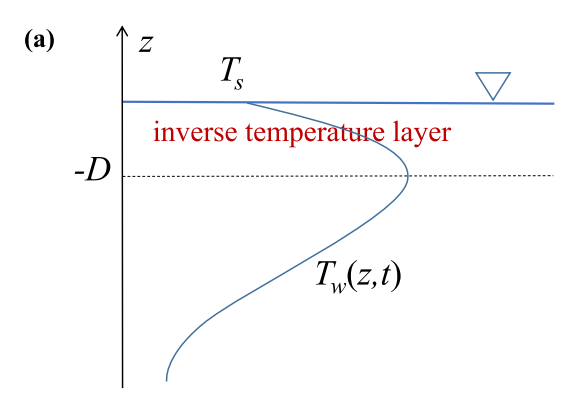
1. Introduction

Solar radiation absorbed by large water bodies such as lakes and oceans is stored in the form of thermal energy as the energy source of longwave radiation and turbulent heat fluxes over the water surfaces (Soloviev & Lukas, 2014). Most of the solar radiation is absorbed within the top water layer of as solar radiation attenuates in water following the Beer's law (e.g., Lee et al., 2014). Observed water temperature tends to decrease with depth (e.g., Peixoto & Oort, 1992), implying that thermal energy (or heat) is transferred from shallower into deeper depth. Meanwhile, heat transfer from water into the atmosphere to balance latent heat (evaporation), sensible heat flux and net longwave radiation loss is only possible when there exists a layer beneath the water-atmosphere interface within which water temperature increases with depth, referred to herein as the "inverse temperature layer" (ITL).

The ITL distinguishes from the "cool-skin," a thin conductive layer on the order of 10^{-3} m or less at the top of oceans (e.g., Saunders, 1967; Soloviev & Schlüssel, 1994, 1996), in two major ways. First, the ITL as a storage of thermal energy has much greater depth than that of cool-skin under common meteorological conditions, for example, wind speed <15-20 m s⁻¹ (Boyle, 2007). Since solar radiation is the dominant energy source, the ITL depth is expected to be comparable to the penetration depth of solar radiation on the order of 10^{-1} to 10^{1} m (Defant, 1961). Field observations of water surface energy budgets (e.g., Liu et al., 2012) have shown that radiation and turbulent heat fluxes over water surface are on the order of 10^{2} W m⁻² with the diurnal variations of water temperature on the order of $1-3^{\circ}$ C. The conserved energy budget requires the ITL depth to be on the order of 10^{0} m, which is consistent with the penetration depth of solar radiation. Second, the heat and momentum transfer within the ITL is driven by wind and thermally induced turbulent mixing while the cool-skin is a conductive layer. Therefore, the ITL depth is expected to have pronounced diurnal and seasonal cycles in response to

WANG ET AL. 1 of 10





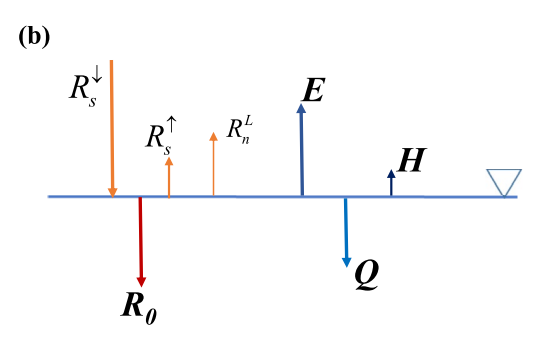


Figure 1. (a) The "inverse-temperature layer" (Inverse temperature layer (ITL)), within which water temperature $T_w(z,t)$ increases with depth (-z), with surface temperature T_s and the ITL depth D. (b) Radiation and heat fluxes at water surface: evaporation (latent heat flux) E, sensible heat flux H (positive into the atmosphere), and water surface heat flux Q (positive away from water surface). R_s^1 (incoming solar radiation), R_s^1 (reflected solar radiation) and R_0 (solar radiation entering water) are positive. R_n^L (net longwave) is defined as positive toward the water-air interface. See water surface energy budget in Equation 1.

solar radiation modulated by wind speed. The ITL also differs in at least two aspects from the warm-layer on the top of ocean (Fairall et al., 1996). First, the ITL has thermally unstable stratification within which temperature increases with depth, while the warm-layer is reportedly stably stratified. Second, the existing observational evidence (reported in this study) indicates the ITL persists at nighttime, while the warm-layer was destroyed by the nighttime convective mixing. Figure 1a shows a conceptual diagram of the ITL of a certain depth below which water temperature either decreases with depth or is possibly nearly uniform within the mixed layer.

The theoretical prediction of the ITL can be verified using the observations of water temperature profile at high resolution (e.g., $\sim 10^{-1}$ m). Even though high resolution in situ measurements of water temperature of the top 10^{-1} to 101 m layer are uncommon, earlier observational studies provided circumstantial evidence of the ITL (Fairall et al., 1996; Keister & Tuttle, 2013; Majidi et al., 2015; Rostad & Kaartvedt, 2013; Vercauteren et al., 2011; Yang et al., 2017) qualitatively consistent with the theoretical prediction. A physically based model also predicts the existence of the ITL with depth on the order of 100 m (Kirillin et al., 2021). Existing observations of water temperature of inland lakes suggest that the ITL is persistent at daily to monthly scales with depths on the order of 100-101 m. Since solar radiation attenuates exponentially with depth according to the Beer's law, water temperature gradient ought to be greater near the surface than at deeper depth. This study reports direct evidence of the ITL, its diurnal and seasonal variations and the corresponding water surface heat flux using the field data of higher resolution water temperature from an inland lake (Liu et al., 2009, 2012, 2016; Zhang & Liu, 2014). Since water surface heat flux cannot be measured directly, the ITL based estimates of water surface heat flux is validated against two physics-based models.

2. Data and Methods

2.1. Field Data

A 5-m flux tower assembled at Ross Barnett Reservoir (hereafter the reservoir), Ridgeland, Mississippi $(32^{\circ}26'N, 90^{\circ}02'W)$ provides the eddy-covariance

(EC) and micrometeorological measurements (Figure S2 in Supporting Information S1). The reservoir has a surface area of \sim 134 km² and water depth of 4–8 m. The distance from the tower to the shore ranges from 2 to \sim 14 km thereby satisfying footprint requirements for EC flux measurements (Liu et al., 2012). An EC system installed at 2.8 m above the water surface consists of a sonic anemometer and an open path CO_2/H_2O infrared gas analyzer. A datalogger recorded 10 Hz 3D wind velocities, temperature and CO_2 and water vapor density. Other meteorological measurements include four components of radiation at 1.2 m, air temperature and relative humidity at 1.9, 2.8, 3.3, 4.0, and 5.2 m, and wind speed and direction at 5.2 m with additional wind speed at 3.3 and 4.0 m. An infrared temperature sensor was deployed to measure water skin temperature T_s . Ten water temperature T_w probes attached to a buoy are placed at 0.5, 1.0, 1.5, 1.8, 2.5, 3.0, 3.5, 4.0, and 4.5 m depth.

2.2. Models of Water Surface Heat Flux Q

Q (Figure 1), like its counterpart ground heat flux at land surface, cannot be measured directly. Q obtained using the eddy-covariance method (e.g., Berg et al., 2020) as an approximation is uncommon. The flux tower at the reservoir is not equipped with an underwater EC system. Therefore, the models of Q are needed for monitoring and simulating the water surface energy budget. The newly formulated ITL based Q described in Section 4 belowviewed as "observed" Q in this study is validated using two well tested models (Wang et al., 2014), namely the Maximum Entropy Production (MEP) and Half-Order-Derivative (HOD) model formulated based on entirely different theories. The MEP and HOD model predict Q from instantaneous and time-history records of radiation

WANG ET AL. 2 of 10



fluxes and water surface temperature, respectively. The two model are referred to as non-gradient models of heat fluxes since they do not use temperature gradient data.

The MEP model predicts the full energy budget of water surface (Q, E, H) in Figure 1) (e.g., Soloviev & Lukas, 2014),

$$\begin{cases} R_0 = R_s^{\downarrow} - R_s^{\uparrow} \\ R_n^L = E + H + Q \end{cases}$$
 (1)

where $R_0(\ge 0)$ is the solar radiation entering water body, R_s^{\downarrow} and R_s^{\uparrow} the incoming and reflected solar radiation, R_n^L the net long-wave radiation, E latent heat flux (evaporation or condensation) and H sensible heat flux. The MEP solution of E, H, Q is expressed as,

$$\begin{bmatrix} 1 + B(\sigma) + \frac{B(\sigma)}{\sigma} \frac{I_w}{I_0 |H|^{\frac{1}{6}}} \end{bmatrix} H = R_n$$

$$E = B(\sigma)H$$

$$Q = R_n^L - E - H$$

$$B(\sigma) \equiv 6 \left(\sqrt{1 + \frac{11}{36}\sigma} - 1 \right), \sigma \equiv \frac{\lambda^2}{R_v c_p} \frac{q_s}{T_s^2}$$
(2)

where $R_n \equiv R_s^{\downarrow} - R_s^{\uparrow} + R_n^{L}$ is net radiation, I_w the thermal inertia of liquid water, I_0 the thermal inertia of (turbulent) air (Wang & Bras, 2009), $T_s \equiv T_w(z=0,t)$ the water surface temperature, $q_s = q^{\text{sat}}(T_s)$ the saturation specific humidity at T_s , λ the latent heat of vapourization of liquid water (2.5 × 10⁶ J kg⁻¹), R_v the gas constant of water vapor (461 J K⁻¹ kg⁻¹) and c_p the specific heat of air at constant pressure (1,004 J K⁻¹ kg⁻¹). $B(\sigma)$ in Equation 2 is the reciprocal Bowen ratio and σ is a dimensionless coefficient characterizing the relative role of water availability (i.e., specific humidity) and temperature in the partition of radiation fluxes into theraml heat fluxes.

The MEP theory (Wang & Bras, 2009) introduces a "dissipation function" in terms of the turbulent/conductive heat fluxes to characterize the state of non-equilibrium system through parameterizing the boundary layer turbulence using the similarity theory (e.g., Arya, 1988). The heat fluxes are obtained by minimizing the dissipation function under the constraint of surface energy balance (e.g., Equation 1). The MEP model does not use wind speed and surface roughness as the model parameters. This is made possible by the parameterization of I_0 in Equation 3 based on the extremum solution of the Monin-Obukhov similarity equations (Wang & Bras, 2010).

The HOD model of Q is formulated based on an analytical solution of the heat transfer equation for the conductive layer of cool-skin (Berg et al., 2020; Kaiser & Williams, 1974; Soloviev & Schlüssel, 1996) expressed as a functional of the time-history of R_0 and $T_w(0, t)$ under the condition of moderate wind speed (e.g., $<15-20 \text{ m s}^{-1}$),

$$Q = \frac{I_w}{\sqrt{\pi}} \int_0^t \frac{\partial T_w(0,\tau)}{\partial \tau} \frac{d\tau}{\sqrt{t-\tau}} - \left(\sum_{i=1}^N F_i \frac{\sqrt{\kappa}}{\varsigma_i}\right) \frac{1}{\sqrt{\pi}} \int_0^t \frac{R_0(\tau)d\tau}{\sqrt{t-\tau}} + \int_0^t \sum_{i=1}^N F_i \left\{\frac{\kappa}{\varsigma_i^2} \exp\left(\frac{\kappa(t-\tau)}{\varsigma_i^2}\right) \operatorname{erfc}\left(\frac{\sqrt{\kappa(t-\tau)}}{\varsigma_i}\right)\right\} R_0(\tau)d\tau$$
(3)

where τ is the integration variable, κ the thermal diffusivity of liquid water, and F_i , ς_i the coefficients in the generalized Beer's law for the attenuation of solar radiation in seawater (Figure S1 in Supporting Information S1),

$$I_B(z) = \sum_{i=1}^{N} F_i \exp\left(\frac{z}{\varsigma_i}\right), z \le 0$$
 (4)

where -z is the depth below water surface. The integration starts from the time ($\tau = 0$) when water temperature profile is close to uniform (vanishing Q). The parameters F_i , ς_i for sea water (Defant, 1961) have been used previously (e.g., Paulson & Simpson, 1981; Wang et al., 2014). The first term on the right-hand-side of Equation 3 is known as the half-order-(time) derivative of $T_w(0,t)$ (e.g., Miller & Ross, 1993), which this non-gradient model is named after.

WANG ET AL. 3 of 10



The HOD model of Q avoids the temperature gradient formula of heat flux by relating the spatial variation of temperature to temporal variation of temperature at the same location of the heat flux (e.g., Wang & Bras, 1999). Similar to the MEP model, the HOD model of Q does not use wind speed and surface roughness as model parameters assuming negligible divergence of horizontal advection within the conducive layer of cool-skin. Q in Equation 3 is mathematically independent of the parameterization of the atmospheric boundary layer turbulence. The non-gradient formulation of Q does not need the data of below water surface temperature. Both MEP and HOD model does not include empirical tuning parameters.

3. Observational Evidence of ITL

Direct evidence of the ITL comes from temperature increasing with depth from water surface and then decreasing with depth. The observed water temperature profiles shown in Figure 2 (and Figures S3–S6 in Supporting Information S1) indicate that the ITL was persistent through the period from 24 August 2007 to 5 March 2008. For example, water surface temperature $T_w(z=0) \equiv T_s$ (Figure 2b) is consistently lower than water temperature at 0.5 m depth, $T_w(0.5)$, measured by the histogram (Figure 2c) with 93.6% of the times $T_w(0.5m) - T_s > 0$. During the period of 08/24/2007 to 01/08/2008, $T_w(0.5m) - T_s > 0$ was observed 90.8% of the observation times (half-an-hour sampling interval). Meanwhile, $T_w(0.5)$ is always higher than water temperature at 1.0 m $T_w(1.0)$ indicated by the corresponding histogram of $T_w(0.5) - T_w(1.0) > 0$ (Figure 2d). The observed water temperature profiles imply that the ITL depth D is 0 < D < 1 m, while T_w below 1.0 m decreases with depth $T_w(1.0) - T_w(1.5, 2.5, 3.5, 4.5) \ge 0$. The temperature difference across the ITL is on the order of $T_w(0.5) - T_w(0.5)$ is greater for the winter months ($T_w(0.5) - T_w(0.5) - T_w(0.5)$) is greater for the winter months ($T_w(0.5) - T_w(0.5) - T_w(0.5)$) is greater for the winter months ($T_w(0.5) - T_w(0.5) - T_w(0.5) - T_w(0.5) - T_w(0.5) > 0$ during the field experiment period do not necessarily imply the disappearance of the ITL. Instead, they are likely caused by shallower ITL depth $T_w(0.5) - T_w(0.5) - T_w(0.5) - T_w(0.5)$ discussed in Section 4.

The monthly mean diurnal cycles of T_w profiles are illustrated in Figure 3 with the corresponding mean diurnal cycles of solar radiation and wind speed in Figure S7 in Supporting Information S1. The ITL has consistent (mean) diurnal cycle from summer to winter season. The ITL T_w reaches diurnal peak around 3 p.m. and solar radiation peaks at local noon, while reaches diurnal low around sunrise time. This behavior is similar to that of surface soil temperature (e.g., Wang & Bras, 1999). Shallower ITL (i.e., 0 < D < 0.5 m) when $T_w(D) > T_s > T_w(0.5)$ mostly occurring between 10 a.m. and 6 p.m. (local time) throughout the observation period is evidenced by 80% of the times when $T_s - T_w(0.5) > 0$ (occurring less than 10% of the times during 08/24/2007–01/08/2008) are during daytime hours. Similar diurnal variations of T_w below 1 m depth (Figure 3) further confirms the dominant role of solar radiation in the seasonal variation of the ITL. Unlike solar radiation, wind speed did not have consistent diurnal cycle (Figure S6 in Supporting Information S1) even though lake breeze with diurnal cycle is expected (wind direct data not available). The intensity of the lake breeze, a type of mesoscale circulations driven by land surface heterogeneity (Pielke et al., 1991; Rotunno, 1983), is reduced by synoptic wind (Wang et al., 1996). Frequent synoptic and/or local convective weather systems passing through the reservoir area tend to suppress the lake breeze. Therefore, persistent diurnal cycle of the ITL through the seasons (Figure 3) with irregular diurnal variation of wind speed (Figure S6 in Supporting Information S1) suggests that wind speed plays a secondary role relaive to that of solar radiation in the ITL dynamics. Further analysis of the effect of lake breeze on the ITL dynamics will be possible when wind directin data become available. Quantitative analysis of the wind-driven turbulence and the formation of the ITL requires physics-based turbulence models beyond the scope of this study. The initial results of an on-going modeling study indicate that the ITL dynamics can be captured by a heat transfer model with the input data of solar radiation and water surface temperature without using wind speed data, suggesting that the effect of wind speed on the ITL were through water surface temperature resulting from water-atmosphere interaction.

Even though wind driven turbulent mixing tends to reduce water temperature gradient, diurnally and seasonally persistent ITL (Figures 2 and 3 and Figures S3–S7 in Supporting Information S1) under various wind conditions implies that the ITL dependent Q (Section 4) is the continuous energy supply of longwave radiation and turbulent fluxes over water surface. The modeling analysis of Q below further reveals that the effect of wind on the ITL is well represented by water surface temperature as the modeled Q are in close agreement with the ITL based estimate of Q without using wind speed data.

WANG ET AL. 4 of 10



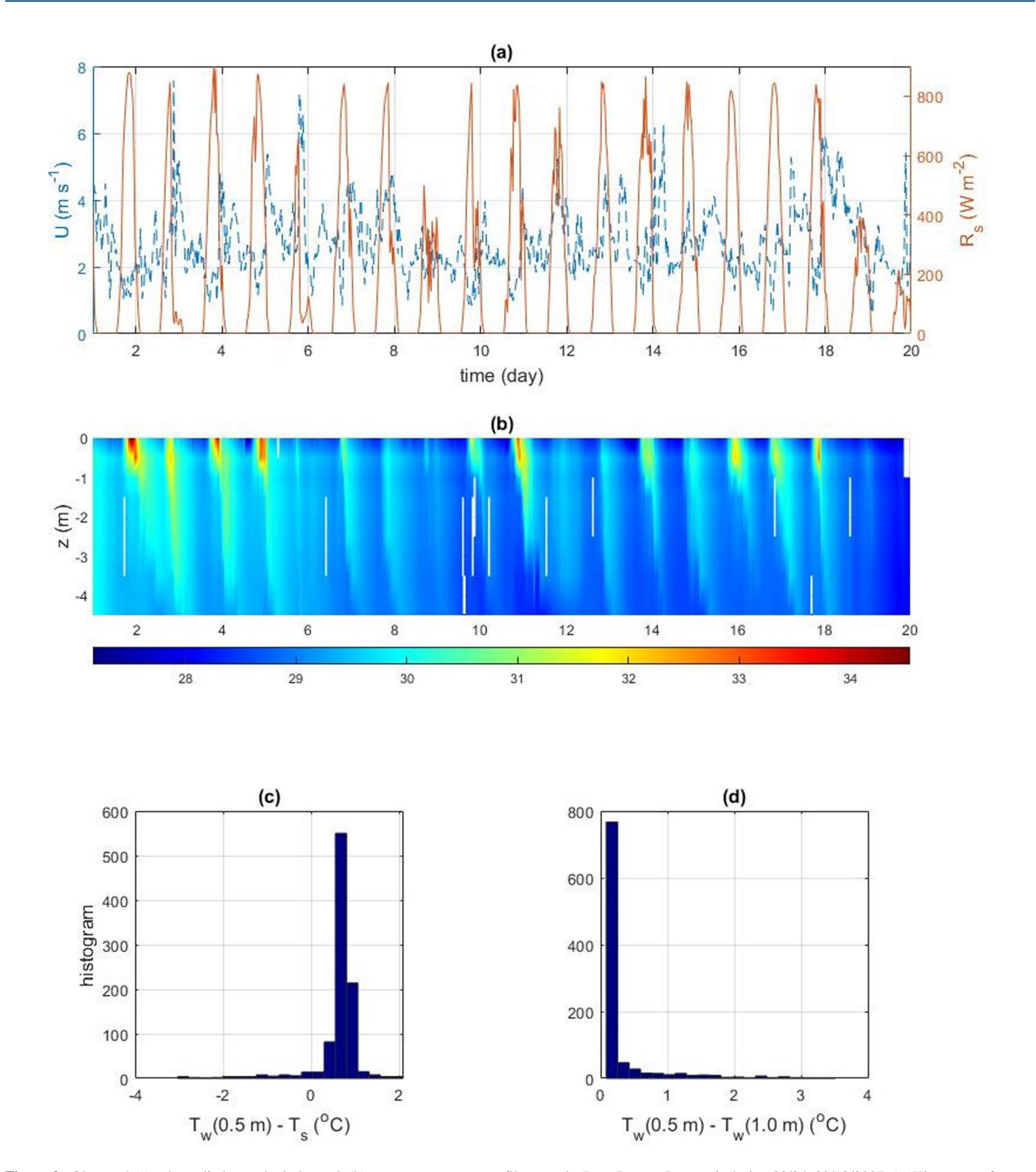


Figure 2. Observed (a) solar radiation and wind speed, (b) water temperature profile T_w at the Ross Barnett Reservoir during 08/24-09/13/2007. (c) Histogram of $T_w(0.5\text{m}) - T_s$ with positive values corresponding to the Inverse temperature layer (ITL). (d) Histogram of $T_w(0.5\text{m}) - T_w(1.0\text{m}) > 0$ indicating the ITL depth between 0.5 and 1.0 m.

WANG ET AL. 5 of 10



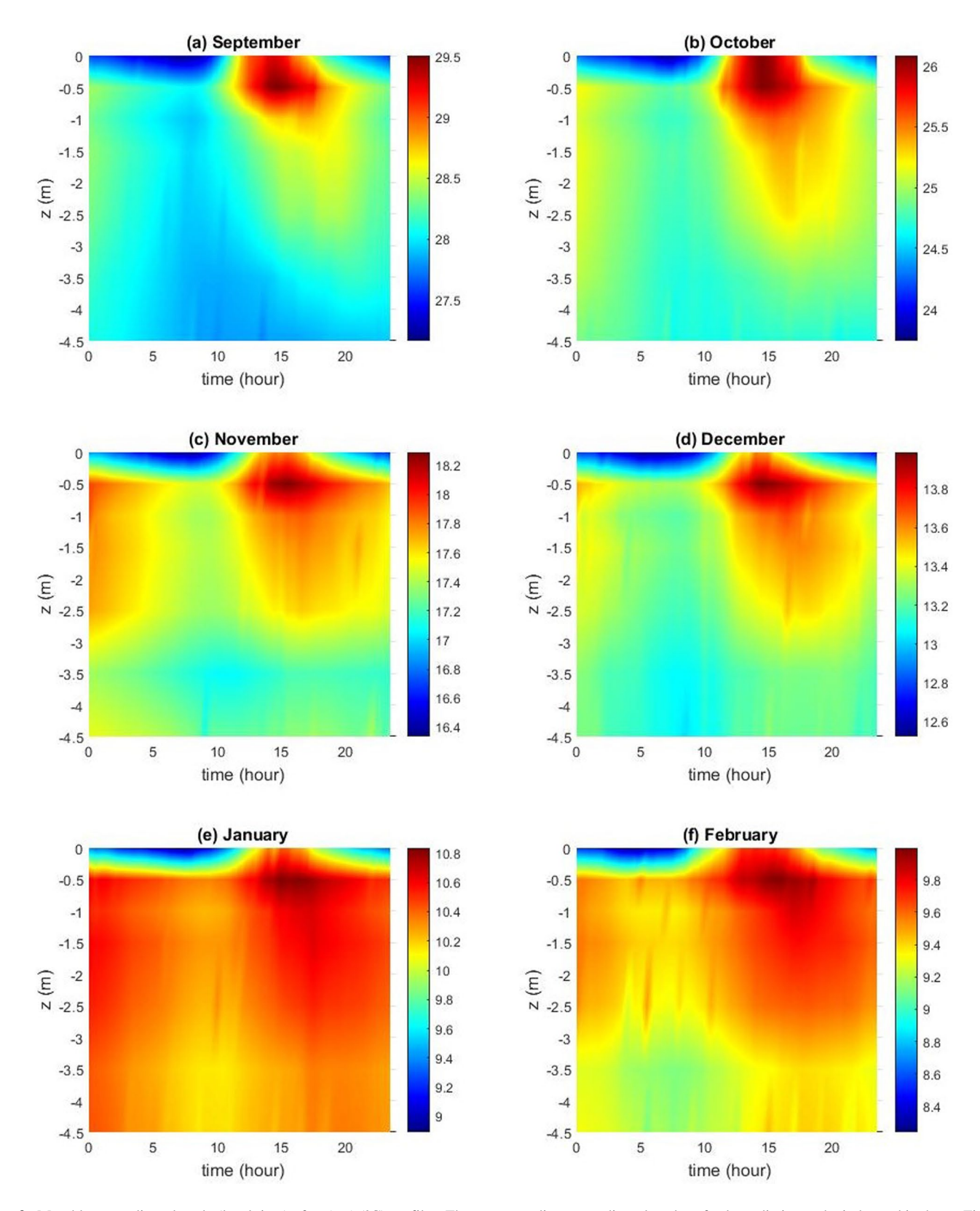


Figure 3. Monthly mean diurnal cycle (local time) of $T_w(z,t)$ (°C) profiles. The corresponding mean diurnal cycles of solar radiation and wind speed is shown Figure S7 in Supporting Information S1.

WANG ET AL. 6 of 10



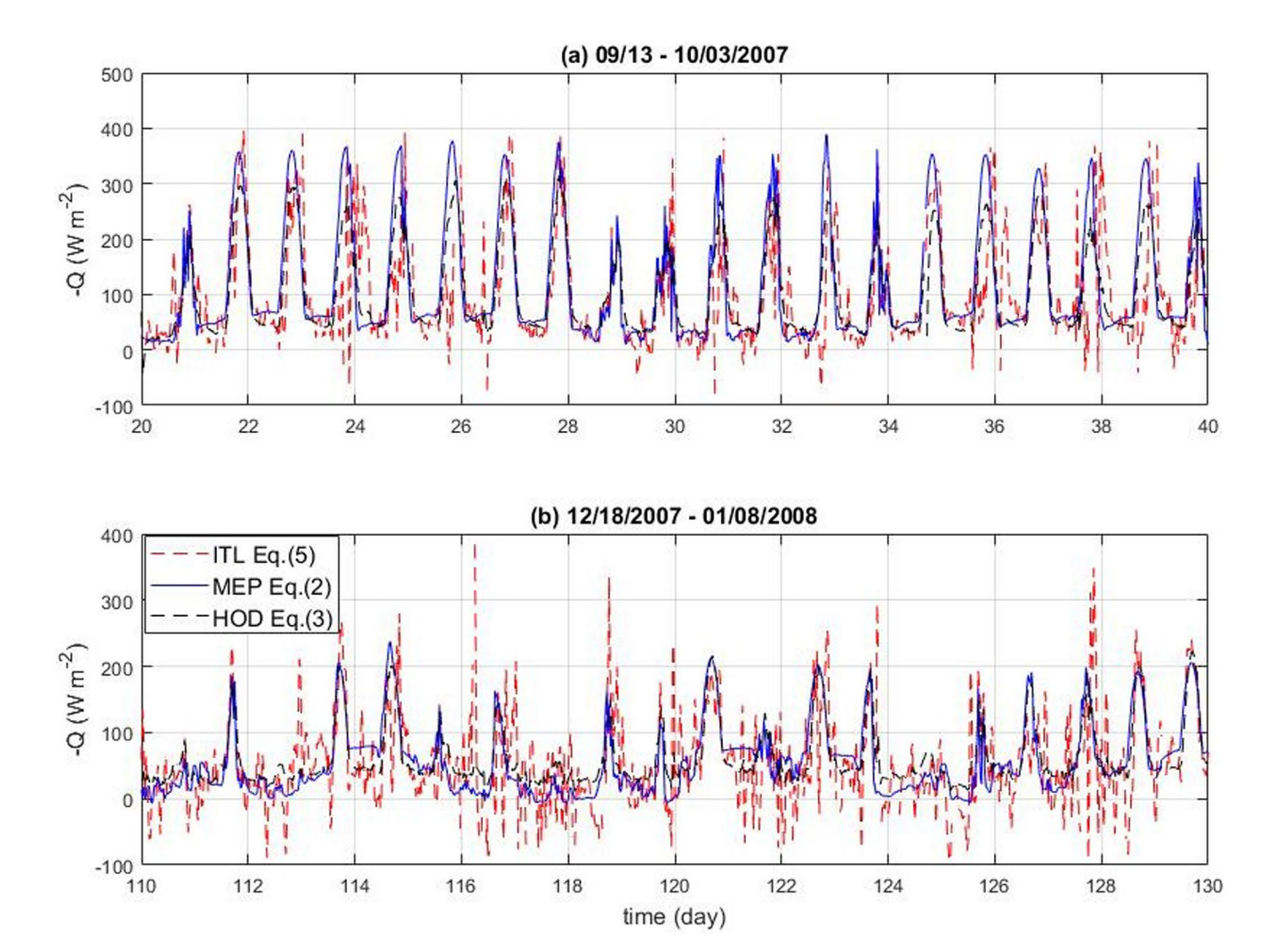


Figure 4. Inverse temperature layer based Q in Equation 2 versus the Maximum Entropy Production Q in Equation 3 and the HOD Q in Equation 4 for (a) summer and (b) winter month. Positive -Q indicates heat transfer from the lake into the atmosphere.

4. ITL and Water Surface Heat Flux

The heat storage change of the ITL poses a constraint on the surface energy budget (Figure 1b) as it is the energy supply of (net) longwave radiation and turbulent heat fluxes at water surface. Water temperature profile $T_w(z,t)$ and solar radiation with zero water heat flux corresponding to vanishing temperature gradient at the bottom of the ITL (Figure 1a) lead to an expression of Q according to the energy conservation of the ITL assuming negligible divergence of horizontal advection,

$$Q = C_w \frac{d}{dt} \int_{-D}^{0} T_w(z, t) dz - R_0 [1 - I_B(-D)]$$
 (5)

where the first term on the right-hand-side is the time change rate of the ITL heat storage, $I_B(z)$ a function characterizing the attenuation of solar radiation in water (Kirillin et al., 2021; Soloviev & Lukas, 2014), and C_w (4.2 × 10⁶J K⁻¹m⁻³) the heat capacity of water. Since direct measurements of underwater solar radiation is not available, a paprameterization of $I_B(z)$ in Equation 4 is used in this study for the estimation of underwater solar radiation. Q coupling the water surface energy budget Equation 1 and the ITL (water body) energy budget Equation 5 reveals that solar radiation is the energy supply of turbulent heat fluxes and net longwave radiation over water surface.

Q in Equation 5 using water temperature and solar radiation data collected at the reservoir has evident diurnal and seasonal cycles (Figure 4). One noticeable feature is the heat transfer from water body into the atmosphere

WANG ET AL. 7 of 10



indicated by positive -Q (also see Figure S7 in Supporting Information S1). Due to limited resolution of water temperature measurements, the ITL depth D is taken as 0.5 m and the integral of $T_w(z,t)$ on the right-hand-side of Equation 5 is approximated as the mean of water temperature at z=0,0.5,1.0 m multiplied by D=0.5 m. The time derivative is computed using a central finite difference of 1 hour interval. Since underwater solar radiation was not measured at the reservoir, a generalized Beer's law function (Equation 4 with the parameters given in Table 2 of Wang et al. (2014)) is used as a surrogate with $I_B(-0.5) \approx 0.5$ (Figure S1 in Supporting Information S1). The uncertainty in the estimated D and the relatively coarse resolution of water temperature measurements are presumably responsible for the noisy estimates of half-an-hourly Q especially during winter months (Figure 4).

The diurnal cycle of Q has greater magnitude during daytime than night-time. The daytime -Q is on the order of $\sim 200-400 \,\mathrm{W} \,\mathrm{m}^{-2}$ dominated by R_0 , the second term on the right-hand-side of Equation $5 \sim 100-400 \,\mathrm{W} \,\mathrm{m}^{-2}$. The magnitude of nighttime Q is on the order of $\sim 50 \mathrm{W m^{-2}}$ when solar radiation vanishes. The ITL temperature increases twice as fast during the day as it decreases during the night. The amplitude of diurnal variations of $T_w(z,t)$ at z=0,0.5,1.0 m is $\sim 1-5^{\circ}$ C (Figure 2 and Figures S3–S5 in Supporting Information S1). Summer time -Q (Figure 4a) is about twice as large as winter time -Q (Figure 4b), which is apparently caused by the seasonal cycle of solar radiation (Figure S7 in Supporting Information S1). One possible cause of the spurious fluctuations in Q and the unrealistically large negative -Q during the winter months (Figure 4b) is the uncertainties of the estimated D due to relatively coarse resolution of water temperature measurements and lack of underwater solar radiation measurements. The uncertainty of $I_B(D)$ may also contribute to the noisy Q since the absorption of solar radiation is affected by water turbidity and the attenuation of solar radiation may deviate from that in Equation 4. Use of measured underwater solar radiation will reduce the uncertainty of Q obtained from Equation 5. Nonetheless, the diurnal and seasonal variations of Q highlight the controlling role of the ITL in water surface energy budget dominated by solar radiation. This is clearly demonstrated in the daily mean Q, wind speed and solar radiation (Figure S7 in Supporting Information S1). The seasonal variation of daily mean Q follows closely that of daily mean solar radiation decreasing from summer to winter, while daily mean wind speed does not have apparent decreasing trend from summer to winter (Figure S7a in Supporting Information S1). The ITL based estimates of Q (Figure 4) are consistent with the MEP and HOD model simulations for the entire period and the agreement between them is even closer at daily scale (Figure S7 in Supporting Information S1). The three different estimates of Q predict persistent heat transfer from water body into the atmosphere (i.e., -Q > 0).

The ITL based, MEP and HOD Q of magnitude ~200 W m⁻² does not support the possibility of disappearing ITL hinted by the events of $T_w(0) - T_w(0.5) > 0$ (Figure 2). When $T_w(0) - T_w(0.5) > 0$ occurred corresponding to $|Q| \sim 200$ W m⁻² during day-time, the ITL tends to be shallower, that is, 0 < D < 0.5 m. The available data suggest that the shallow ITL of the reservoir with 0 < D < 0.5 m was a frequent occurrence for at least ~10% of the period of 08/24/2007 to 03/05/2008. Detection of the diurnal cycles of shallower ITL (e.g., <0.5 m) requires even higher resolution (e.g., ~5 cm) data of the top-layer water temperature.

5. Discussions

The ITL dynamics and Q strongly depend on not only solar radiation at water surface but also its attenuation in water body. The agreement of the HOD modeled (Equation 3) with the ITL based and MEP modeled Q (Figure 4; Figure S7 in Supporting Information S1) is achieved when the attenuation of solar radiation in water is described by I_B in Equation 4, which has a sharp gradient near the water surface corresponding to strong absorption within a thin top layer of depth (<10 cm) (Figure S1 in Supporting Information S1). In contrast, a single-band exponential attenuation profile I_R (Equation 1 in Kirillin et al., 2021), corresponds to weaker and more gradual absorption of solar radiation in the top-layer. Use of a single-band attenuation function in the HOD model leads to substantial biases in the HOD modeled Q compared to the ITL based and MEP modeled Q (not shown). The fact that I_B in Equation 4 in the HOD model also simulates ocean surface heat flux in close agreement with the MEP model (Wang et al., 2014) indicates that I_B originally formulated for seawater is a good approximation for freshwater, justifying the generality of this parameterization of solar radiation attenuation in water. Meanwhile, water turbidity may vary causing uncertainty of the attenuation coefficients (F_t , ς_t in Equation 4) that need to be estimated more accurately using the measurements of underwater solar radiation.

The heat storage of the ITL is the energy supply of the water surface longwave radiation (loss) and turbulent heat fluxes. The inverse temperature gradient (i.e., temperature increasing with depth) of the ITL ensures heat transfer from water body into the atmosphere. The magnitude of water heat flux (|Q|) is limited by the depth and

WANG ET AL. 8 of 10



temperature change rate of the ITL. According to Equation 5, nighttime |Q| is much smaller than the daytime |Q| due to vanishing solar radiation. Limited amplitude of diurnal temperature variation (\sim 2–3°C) and ITL depth (\sim 1 m) further constrains |Q| hence the heat transfer into the atmosphere especially during nighttime. This is consistent with the observations that |Q| is substantially higher even though the ITL depth is shallower during daytime, indicating the dominant role of solar radiation in |Q|. More accurate estimation of |Q| can be achieved using high resolution measurements of water temperature and underwater solar radiation.

The unstable thermal stratification of the ITL is maintained under opposite forcings. The cooling effect of long-wave radiation and evaporation at water surface tend to produce unstable thermal stratification, while the absorption of solar radiation in water tends to produce stable thermal stratification. The wind-induced (mechanical) mixing tends to reduce the ITL temperature gradient. Therefore, stronger wind does not necessarily enhance |Q| indicated by the relatively weak correlation between Q (and turbulent heat fluxes) and wind speed (e.g., Figure S7 in Supporting Information S1). Shallower daytime ITL corresponding to strong solar heating and stronger radiative and/or evaporative cooling obscures the effect of wind-induced mixing on Q. Understanding of the interaction between solar heating, radiative/evaporative cooling and wind-induced mixing and its impact on the ITLdynamics and Q needs high-fedelity model (e.g., large-eddy simulation models for water boundary-layer) simulations with realistic water surface boundary conditions from in situ observations. This should be a focus of future research. Future research should also include an quantitative analysis of the diurnal and seasonal variation of the ITL (e.g., depth) using higher resolution (e.g., \sim 0.05 m) and longer duration (e.g., 1-3 years) data of water temperature profile (e.g., Mor et al., 2018) and other meteorological variables such as underwater solar radiation profile.

6. Conclusions

The theoretical prediction of the inverse-temperature layer (ITL) over natural water bodies is supported by the observations obtained from an inland lake. The ITL with depth up to one m persists year-round under all wind conditions. The ITL tends to be shallower during daytime than nighttime. Heat transfer from the water body into the atmosphere corresponds to water surface heat flux up to \sim 600 W m⁻² during summer daytime and \sim 50 W m⁻² during nighttime. Water surface heat flux simulated using two non-gradient models are consistent with the ITL based estimates with evident diurnal and seasonal cycle following those of solar radiation. The ITL and water surface heat flux depend on both solar radiation at water surface and its attenuation profile in water body. Further quantitative analysis of the ITL dynamics needs high resolution (e.g., \sim 5 cm) measurements of water temperature and underwater solar radiation profile.

Data Availability Statement

The data used in this study is publicly available from https://doi.org/10.5281/zenodo.7179025.

Acknowledgments References

National Science Foundation Hydrological Sciences and Physical and Berg, F

Dynamic Meteorology Program Grants EAR-2006281 (Georgia Institute of Technology), EAR-2002644 (Washington State University), and EAR-2003076 (University of Minnesota).

This study is jointly sponsored by the

Arya, S. P. (1988). Introduction to micrometeorology. Academic Press.

Berg, P., Pace, M. L., & Buelo, C. D. (2020). Air–water gas exchange in lakes and reservoirs measured from a moving platform by underwater eddy covariance. *Limnology and Oceanography: Methods*, 18(8), 424–436. https://doi.org/10.1002/lom3.10373

Boyle, J. P. (2007). Field results from a second-generation ocean/lake contact heat flux, solar irradiance, and temperature measurement instruments—The multi-sensor float. *Journal of Atmospheric and Oceanic Technology*, 24(5), 856–976. https://doi.org/10.1175/JTECH1898.1 Defant, A. (1961). *Physical oceanography* (Vol. 1, p. 729). Pergamon.

Fairall, C. W., Bradley, E. F., Godfrey, J. S., Wick, G. A., Edson, J. B., & Young, G. S. (1996). Cool-skin and warm-layer effects on sea surface temperature. *Journal of Geophysical Research*, 101(C1), 1295–1308. https://doi.org/10.1029/95jc03190

Kaiser, J. A. C., & Williams, K. G. (1974). Measurement of the vertical heat flux in the upper ocean layer. *Journal of Physical Oceanography*, 4(2), 137–114. https://doi.org/10.1175/1520-0485(1974)004<0137:MOTVHF>2.0.CO;2

Keister, J. E., & Tuttle, L. B. (2013). Effects of bottom-layer hypoxia on spatial distributions and community structure of mesozooplankton in a sub-estuary of Puget Sound. Limnology & Oceanography, 58(2), 667–680. https://doi.org/10.4319/lo.2013.58.2.0667

Kirillin, G. B., Shatwell, T., & Wen, L. (2021). Ice-covered lakes of Tibetan Plateau as solar heat collectors. *Geophysical Research Letters*, 48(14), e2021GL093429. https://doi.org/10.1029/2021GL093429

Lee, Z., Shang, S., Du, K., Wei, J., & Arnone, R. (2014). Useable solar radiation and its attenuation in the upper water column. *Journal of Geophysical Research - Oceans*, 119(2), 1488–1497. https://doi.org/10.1002/2013JC009507

Liu, H., Zhang, Q., & Dowler, G. (2012). Environmental controls on the surface energy budget over a large southern inland water in the United States: An analysis of one-year eddy-covariance flux data. *Journal of Hydrometeorology*, 13(6), 1893–1910. https://doi.org/10.1175/ JHM-D-12-020.1

Liu, H., Zhang, Q., Katul, G. G., Cole, J. J., Chapin, F. S., III., & MacIntyre, S. (2016). Large CO₂ effluxes at night and during synoptic weather events significantly contribute to CO₂ emissions from a reservoir. *Environmental Research Letters*, 11(6), 64001. https://doi.org/10.1088/1748-9326/11/6/064001

WANG ET AL. 9 of 10



- Liu, H., Zhang, Y., Liu, S., Jiang, H., Sheng, L., & Williams, Q. L. (2009). Eddy covariance measurements of surface energy budget and evaporation in a cool season over southern open water in Mississippi. *Journal of Geophysical Research: Atmosphere*, 114(D4), D04110. https://doi.org/10.1029/2008JD010891
- Majidi, M., Alizadeh, A., Farid, A., & Vazifedoust, M. (2015). Estimating evaporation from lakes and reservoirs under limited data condition in a semi-arid region. *Water Resources Management*, 29(10), 3711–3733. https://doi.org/10.1007/s11269-015-1025-8
- Miller, K. S., & Ross, B. (1993). An introduction to the fractional calculus and fractional differential equations. Wiley.
- Mor, Z., Assouline, S., Tanny, J., Lensky, I. M., & Lensky, N. G. (2018). Effect of water surface salinity on evaporation: The case of a diluted buoyant plume over the Dead Sea. Water Resources Research, 54(3), 1460–1475. https://doi.org/10.1002/2017WR021995
- Paulson, C. A., & Simpson, J. J. (1981). The temperature difference across the cool skin of the ocean. *Journal of Geophysical Research*, 86(C11), 11044–11054. https://doi.org/10.1029/JC086iC11p11044
- Peixoto, J. P., & Oort, A. H. (1992). Physics of climate. American Institute of Physics.
- Pielke, R. A., Dalu, G. A., Snook, J. S., Lee, T. J., & Kittel, T. G. F. (1991). Nonlinear influence of mesoscale land use on weather and climate. *Journal of Climate*, 4(No. 11), 1053–1069. https://doi.org/10.1175/1520-0442(1991)004<1053:niomlu>2.0.co;2
- Rostad, A., & Kaartvedt, S. (2013). Seasonal and diel patterns in sedimentary flux of krill fecal pellets recorded by an echo sounder. Limnology & Oceanography, 58(6), 1985–1997. https://doi.org/10.4319/lo.2013.58.6.1985
- Rotunno, R. (1983). On the Linear Theory of the land and sea breeze. *Journal of the Atmospheric Sciences*, 40(8), 1999–2009. https://doi.org/10.1175/1520-0469(1983)040%3C1999:OTLTOT%3E2.0.CO;2
- Saunders, P. (1967). Temperature at the ocean-air interface. *Journal of the Atmospheric Sciences*, 24(3), 269–273. https://doi.org/10.1175/1520-0469(1967)024<0269:TTATOA>2.0.CO;2
- Soloviev, A. V., & Lukas, R. (2014). The near-surface layer of the ocean. Springer.
- Soloviev, A. V., & Schlüssel, P. (1994). Parameterization of the cool skin of the ocean and of the air-ocean gas transfer on the basis of modeling surface renewal. *Journal of Physical Oceanography*, 24(6), 1139–1346. https://doi.org/10.1175/1520-0485(1994)024<1339: POTCSO>2.0.CO;2
- Soloviev, A. V., & Schlüssel, P. (1996). Evolution of cool skin and direct air-sea gas transfer coefficient during daytime. Boundary-Layer Meteorology, 77(1), 45–68. https://doi.org/10.1007/BF00121858
- Vercauteren, N., Huwald, H., Bou-Zeid, E., Selker, J. S., Lemmin, U., Parlange, M. B., & Lunati, I. (2011). Evolution of superficial lake water temperature profile under diurnal radiative forcing. Water Resources Research, 47(9), W09522. https://doi.org/10.1029/2011WR010529
- Wang, J., & Bras, R. L. (1999). Ground heat flux estimated from surface soil temperature. *Journal of Hydrology*, 216(3–4), 214–226. https://doi.org/10.1016/S0022-1694(99)00008-6
- Wang, J., & Bras, R. L. (2009). A model of surface heat fluxes based on the theory of maximum entropy production. *Water Resources Research*, 45(11), W11422. https://doi.org/10.1029/2009WR007900
- Wang, J., & Bras, R. L. (2010). An extremum solution of Monin-Obukhov similarity equations. *Journal of the Atmospheric Sciences*, 67(2), 485–499. https://doi.org/10.1175/2009JAS3117.1
- Wang, J., Bras, R. L., & Eltahir, E. (1996). A stochastic linear theory of mesoscale circulation induced by the thermal heterogeneity of the land surface. *Journal of the Atmospheric Sciences*, 53(22), 3349–3366. https://doi.org/10.1175/1520-0469(1996)053<3349:ASLTOM>2.0.CO;2
- Wang, J., Bras, R. L., Nieves, V., & Deng, Y. (2014). A model of energy budgets over water, snow, and ice surfaces. *Journal of Geophysical Research: Atmospheres*, 119(10), 6034–6051. https://doi.org/10.1002/2013JD021150
- Yang, J., Wang, Z.-H., Li, Q., Vercauteren, N., Bou-Zeid, E., & Parlange, M. B. (2017). A novel approach for unraveling the energy balance of water surfaces with a single depth temperature measurement. Limnology & Oceanography, 62(1), 89–103. https://doi.org/10.1002/lno.10378
- Zhang, Q., & Liu, H. (2014). Seasonal changes in physical processes controlling evaporation over inland water. *Journal of Geophysical Research: Atmosphere*, 119(16), 9779–9792. https://doi.org/10.1002/2014JD021797

WANG ET AL. 10 of 10